

Understanding Muon Diffusion in Perovskite Oxides below Room Temperature Based on Harmonic Transition State Theory

T. U. Ito

Advanced Science Research Center, Japan Atomic Energy Agency, Tokai, Ibaraki 319-1195, Japan

W. Higemoto

*Advanced Science Research Center, Japan Atomic Energy Agency, Tokai, Ibaraki 319-1195, Japan and
Department of Physics, Tokyo Institute of Technology, Meguro, Tokyo 152-8551, Japan*

K. Shimomura

*Institute of Materials Structure Science, High Energy Accelerator
Research Organization (KEK), Tsukuba, Ibaraki 305-0801, Japan*

(Dated: December 12, 2023)

In positive muon spin rotation and relaxation (μ^+ SR) spectroscopy, positive muons (μ^+) implanted into solid oxides are conventionally treated as immobile spin-probes at interstitial sites below room temperature. This is because each μ^+ is thought to be tightly bound to an oxygen atom in the host lattice to form a muonic analogue of the hydroxy group. On the basis of this concept, anomalies in μ^+ SR spectra observed in oxides have been attributed in most cases to the intrinsic properties of host materials. On the other hand, global μ^+ diffusion with an activation energy of ~ 0.1 eV has been reported in some chemically-substituted perovskite oxides at cryogenic temperatures, although the reason for the small activation energy despite the formation of the strong O μ bond has not yet been quantitatively understood. In this study, we investigated interstitial μ^+ diffusion in the perovskite oxide lattice using KTaO₃ cubic perovskite as a model system. We used the μ^+ SR method and density functional theory calculations along with the harmonic transition state theory to study this phenomenon both experimentally and theoretically. Experimental activation energies for global μ^+ diffusion obtained below room temperature were less than a quarter of the calculated classical potential barrier height for a bottleneck μ^+ transfer path. The reduction in the effective barrier height could be explained by the harmonic transition state theory with a zero-point energy correction; a significant difference in zero-point energies for μ^+ at the positions in the O μ bonding equilibrium state and a bond-breaking transition state was the primary cause of the reduction. This suggests that the assumption of immobile μ^+ in solid oxides is not always satisfied since such a significant decrease in diffusion barrier height can also occur in other oxides.

I. INTRODUCTION

The positive muon spin rotation and relaxation (μ^+ SR) method has been widely used to investigate the microscopic properties of solids.^{1–6} This technique involves implanting spin-polarized positive muons (μ^+) into lattice interstices as microscopic magnetic probes to observe local magnetic fields arising from surrounding electrons and nuclei. This allows for the study of the electronic state of materials from a microscopic point of view, in a manner similar to the nuclear magnetic resonance technique. In most cases, μ^+ SR is used as a silent probe; the implanted μ^+ is assumed to stay at fixed sites and not to alter the electronic properties of the host material. However, in reality, the implanted μ^+ may change local electronic structures and atomic arrangements to some extent due to its positive charge.^{7–11} In addition, μ^+ is relatively mobile in crystalline lattices because of its light mass, which is approximately one ninth that of proton. The diffusion of μ^+ can cause drastic changes in μ^+ SR spectra, such as the narrowing of lines¹² and the averaging of spin precession frequencies,^{13,14} even when host materials do not exhibit any anomalous behavior. Therefore, a deep understanding of both μ^+ diffusion and

the perturbation induced by μ^+ on its surroundings is always necessary for researchers using μ^+ SR spectroscopy, regardless of whether they are interested in such phenomena or not.

The diffusion of μ^+ has been extensively studied in elemental metals and its quantum nature at cryogenic temperatures has been unambiguously established.¹² For instance, anomalous temperature dependencies of an interstitial μ^+ hopping rate in copper were successfully described by a microscopic quantum tunneling model that takes into account interactions between μ^+ and the lattice, and conduction electrons.^{15–19} In contrast, μ^+ implanted into solid oxides is usually regarded as immobile below room temperature because it is thought to be tightly bound to an oxygen atom in the host lattice to form a muonic analogue of the hydroxy group. Many researchers have accepted this assumption and applied μ^+ SR spectroscopy to investigations of magnetism and ion diffusion in oxides, where anomalies appearing in μ^+ SR spectra have simply been interpreted as manifestations of the material's nature.^{20–22} On the other hand, *local* μ^+ hopping has undoubtedly been observed below room temperature in transition-metal oxide antiferromagnets with the corundum structure.^{23,24} Moreover, *global* μ^+ diffusion with an activation en-

ergy of ~ 0.1 eV has been reported in some chemically-substituted perovskite oxides, such as Sc-doped SrZrO_3 ²⁵ and $\text{BaTiO}_{3-x}\text{H}_x$ oxyhydride²⁶, at cryogenic temperatures. While the quantum effect associated with the light mass is inferred to be important in μ^+ diffusion, the reason for the small activation energy despite the formation of the strong $\text{O}\mu$ bond has not yet been quantitatively understood.

In this article, we report μ^+ SR and density functional theory (DFT) calculations studies on μ^+ diffusion in insulating KTaO_3 with a cubic perovskite structure to gain a comprehensive understanding of the μ^+ diffusion in the perovskite oxide lattice. KTaO_3 is an ideal system for investigating the μ^+ diffusion since it has dense nuclear spins and preserves the cubic perovskite structure even at cryogenic temperatures. These features facilitate experimental detection of the μ^+ diffusion and its modeling in DFT calculations. DFT has recently been used extensively to provide valuable information for identifying μ^+ stopping sites and for estimating their stabilities and charge states as hydrogen-like defects in crystalline lattices from a theoretical viewpoint.^{11,21,23,24,27-30} However, the application of DFT to support μ^+ SR data analysis has mostly been limited to a classical level, despite the importance of quantum effects arising from the light mass of μ^+ . A recent DFT study by Onuorah *et al.* highlights the importance of zero-point energies (ZPEs) in finding stable μ^+ sites in metals,³¹ but their impact on μ^+ diffusion has not been discussed in detail. In this study, we handle ZPEs for μ^+ in KTaO_3 within the frameworks of double Born-Oppenheimer and harmonic approximations,³¹ and show how the effective activation barrier for interstitial μ^+ diffusion is lowered due to the difference in ZPEs for μ^+ at positions in the $\text{O}\mu$ bonding equilibrium state and a bond-breaking transition state based on the harmonic transition state theory.^{32,33}

This paper is organized as follows. After a brief description of the experiments in Sec. II, we report our experimental results in Sec. III together with the results of data analysis using the dynamical Gaussian Kubo-Toyabe theory and a two-state model. In Sec. IV and V, we describe computational details and results of DFT calculations performed for providing a semi-quantitative description of long-range interstitial μ^+ diffusion in KTaO_3 below room temperature. In Sec. VI, we discuss the implications of these results for interstitial μ^+ diffusion in oxides with a specific focus on the impact of ZPEs on the effective barrier height for μ^+ hopping. Finally, we summarize our conclusions in Sec. VII.

II. EXPERIMENTAL DETAILS

High-purity (4N) KTaO_3 single crystals of $10 \times 10 \times 0.5$ mm³ were obtained from MTI Corporation, USA. The single crystals were grown by the top-seed flux method and cut along the cubic (001) plane. Time-differential μ^+ SR experiments were per-

formed at Japan Proton Accelerator Research Complex (J-PARC), Japan, and Paul Scherrer Institut (PSI), Switzerland, using a spin-polarized surface muon beam in a longitudinal field configuration with its initial polarization direction nominally parallel to the beam axis. The general purpose μ^+ SR spectrometers at D1 and S1 areas of J-PARC with a conventional ^4He flow cryostat and the Low Temperature Facility μ^+ SR instrument with a ^3He - ^4He dilution refrigerator at PSI were used for the temperature ranges of 3-300 K and 0.1-5 K, respectively. The KTaO_3 single crystals were mounted on a silver sample holder with the (001) plane perpendicular to the beam axis. The asymmetry of μ^+ beta decay, A , was monitored by the “Forward” and “Backward” positron counters as a function of the elapsed time t from the instant of muon implantation.

$A(t)$ can be decomposed into partial asymmetries from muons stopped in the sample, $A_s(t)$, and the silver sample holder, A_{BG} , the latter of which is substantially a time-independent constant. The magnitude of A_{BG} was determined using a reference sample (holmium) with similar geometry to the KTaO_3 sample and it was subtracted from $A(t)$. The remaining $A_s(t)$ was divided by $A_s(t=0)$ to obtain the time-evolution of spin polarization $P(t)$ for muons that stopped in the sample. In this normalized form, μ^+ SR data sets recorded with different spectrometers can be directly compared.

The muons implanted into KTaO_3 depolarize mainly due to dipole-dipole interactions with surrounding ^{181}Ta , ^{39}K , and ^{41}K nuclei having natural abundances of 99.988%, 93.258%, and 6.730%, respectively.³⁴ $P(t)$ in such a dense nuclear spin system can be approximately described by averaging spin precession signals for muons that feel random nuclear dipolar fields with an isotropic Gaussian distribution (local field approximation).³⁵ When muons are immobile in the μ^+ SR time window of up to ~ 20 μs , $P(t)$ in a zero applied field (ZF) is expected to have a Gaussian-like shape, which reflects the Gaussian distribution of the local fields. As the hopping rate of muons increases, the shape of $P(t)$ in ZF should gradually change from the Gaussian-like curve to an exponential-like curve with a decrease in a muon spin relaxation rate (motional narrowing). This behavior can be approximately described with the dynamical Gaussian Kubo-Toyabe (DKT) theory based on a strong collision approximation.³⁵ In a faster diffusion regime, the effects of muon trapping at dilute defects and/or detrapping from them may appear in $P(t)$, which can be approximately expressed using a two-state (2S) model.^{25,26,36,37}

III. EXPERIMENTAL RESULTS

μ^+ SR spectra in ZF exhibit a complicated temperature dependence below room temperature, with the spectral shape changing between Gaussian-like and exponential-like functions (Fig.1(a)). To obtain an overview of the

temperature variation, the spectra were tentatively fitted to a stretched exponential function, $p_0 \exp(-(\Delta t)^\beta)$. The initial polarization p_0 is approximately unity over the entire temperature range (Fig. 1(b)), indicating that almost all the muons implanted into the sample are in diamagnetic environments. The exponent β , which was allowed to vary between 1 and 2, gradually decreases to 1 as the temperature increases from 1 to 10 K (Fig. 1(c)). This is accompanied by a decrease in the muon spin relaxation rate Λ (Fig. 1(d)). This behavior strongly suggests that the hopping motion of μ^+ , which is detectable within the μ^+ SR time window, is activated even below 10 K. Further information on the μ^+ state in this temperature regime can be obtained through curve fitting analysis using a DKT function,³⁵ which is described in Sec. III A.

The exponential-like $P(t)$ at around 10-75 K changes to a Gaussian-like curve toward 135 K with an increase in Λ . Similar behavior has been reported in Sc-doped SrZrO_3 ,²⁵ $\text{BaTiO}_{3-x}\text{H}_x$ oxyhydride,²⁶ ReO_3 ,³⁷ and impurity-doped Nb,³⁶ ascribed to an increasing rate of μ^+ trapping at a dilute defect with increasing temperature. Therefore, this behavior in KTaO_3 can also be regarded as a signature of μ^+ trapping at a dilute defect (defect A) that occurs via long-range interstitial μ^+ diffusion. The exponential-like shape is recovered at around 200 K with a local minimum in Λ , and then the Gaussian-like shape is restored with increasing temperature toward 300 K. The former and latter behavior can be attributed to an increasing rate of μ^+ jumps between defect A through the interstitial diffusion path, and that of μ^+ trapping at another more dilute defect (defect B), respectively. All these processes above 75 K can be approximately expressed using the 2S model, which is described in Sec. III B.

A. Dynamical Gaussian Kubo-Toyabe analysis for $3.5 < T < 25$ K

The DKT function, $G_{\text{DKT}}(t; \Delta, \nu)$, describes the time evolution of muon spin polarization in fluctuating random local fields, which are characterized by the root-mean-square (rms) width of the Gaussian field distribution, $\sigma (= \Delta/\gamma_\mu)$, where γ_μ is the muon gyromagnetic ratio, and the rate of its redistribution, ν . In the present case, ν can be considered as the μ^+ hopping rate since the spins of surrounding Ta and K nuclei are substantially static in the μ^+ SR time window. Even when implanted muons induce fast nuclear spin precession around μ^+ -nuclei axes via electric quadrupole interactions, the nuclear spin components along these axes still produce the static field distribution at μ^+ sites.

We first performed a simultaneous fit of μ^+ SR spectra at 3.5 K under a ZF and a longitudinal field of 1.0 mT to $G_{\text{DKT}}(t; \Delta, \nu)$ and obtained $\Delta = 0.1322(12) \mu\text{s}^{-1}$ (Fig. 2(a)). The experimental value of Δ can be compared with a theoretical value, Δ_{calc} , obtained from a

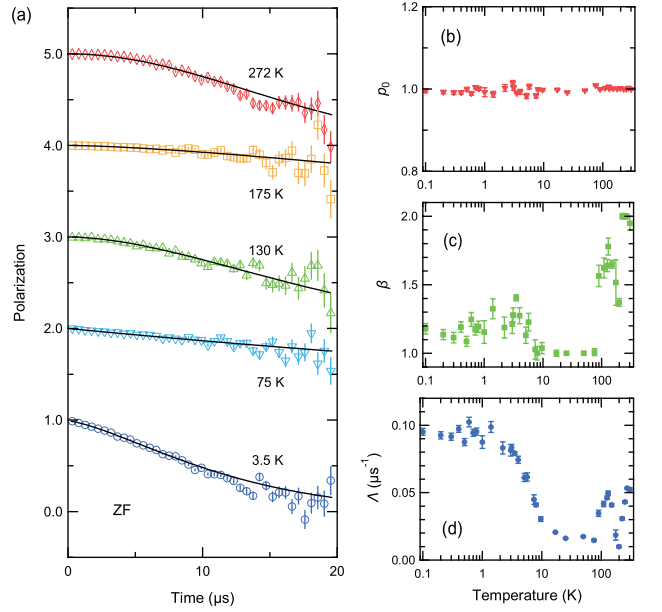


FIG. 1. (a) ZF- μ^+ SR spectra at 3.5, 75, 130, 175, and 272 K, compared to the best fits to the stretched exponential function, $p_0 \exp(-(\Delta t)^\beta)$ (solid curves). For clarity, the base lines are vertically offset by +1 as the temperature increases. Right panels show (b) p_0 , (c) β , and (d) Λ as functions of temperature.

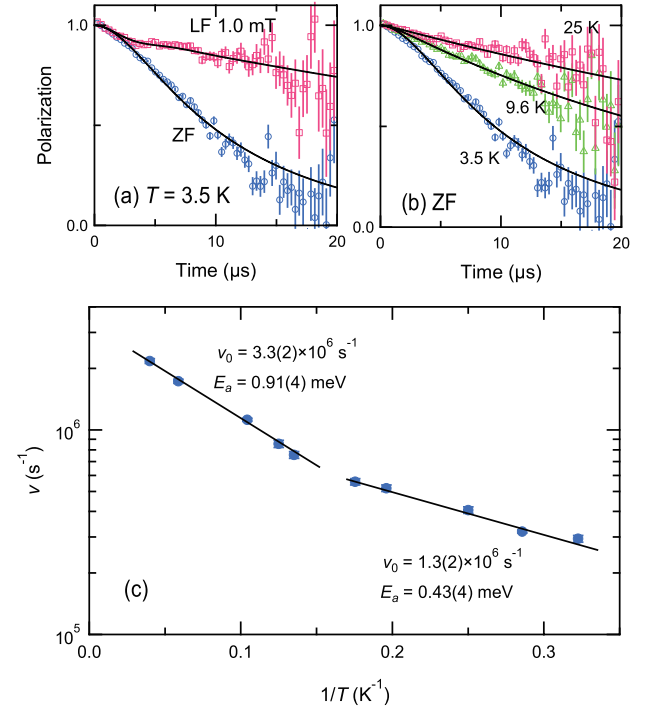


FIG. 2. (a) μ^+ SR spectra at 3.5 K under a ZF and a longitudinal field of 1.0 mT, compared to the result of the simultaneous fit to the DKT function. (b) ZF- μ^+ SR spectra at 3.5, 9.6, and 25 K. Solid curves represent the best fits to the DKT function with Δ fixed to $0.1322 \mu\text{s}^{-1}$. (c) Arrhenius plot of ν . Solid lines represent fits to the Arrhenius-type function.

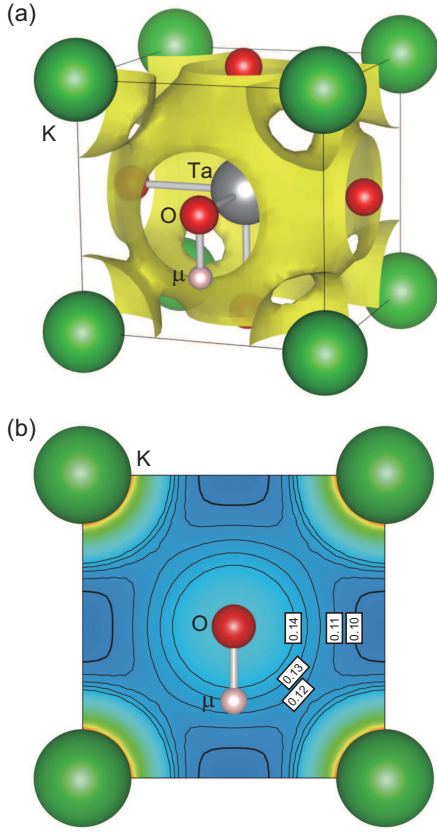


FIG. 3. Spatial distribution of Δ_{calc} in the KTaO_3 lattice. (a) Isosurface for $\Delta_{calc} = 0.13 \mu\text{s}^{-1}$. (b) Contour plot on the face of the cubic cell. The smallest spheres represent the most probable equilibrium position for μ^+ suggested from DFT calculations for a hydrogen interstitial impurity in KTaO_3 .^{33,38}

dipolar sum calculation that takes into account the experimental geometry using the single crystalline sample. Figure 3 shows the spatial distribution of Δ_{calc} in the KTaO_3 lattice. The calculation was performed for the case where μ^+ -induced electric quadrupole interactions on surrounding nuclei are negligible. The most probable equilibrium position for μ^+ suggested by DFT calculations for a hydrogen interstitial impurity in KTaO_3 ^{33,38} is also shown with the smallest sphere, which is very close to the isosurface and contour for $\Delta_{calc} = 0.13 \mu\text{s}^{-1}$. The values of Δ_{calc} for μ^+ at K, Ta, and O vacancies (V_K , V_{Ta} , and V_O) were also calculated for the unrelaxed lattice and tabulated in Table I along with the values of Δ_{calc}^{eq} calculated for the case where the μ^+ -induced electric quadrupole interactions are taken into account for nearest neighbor nuclei. The calculated values for the cation vacancy sites are far from the experimental value, indicating that direct μ^+ trapping at these vacancy sites in the μ^+ deceleration process can be ignored. Based on the good agreement between the experimental and theoretical values of Δ for μ^+ at the interstitial site, we concluded that the as-implanted μ^+ mixture is almost purely composed of the interstitial μ^+ on the face of the cubic

TABLE I. Δ_{calc} and Δ_{calc}^{eq} for μ^+ at V_K , V_{Ta} , V_O , and the interstitial position shown in Fig. 3.

Muon site	$\Delta_{calc} (\mu\text{s}^{-1})$	$\Delta_{calc}^{eq} (\mu\text{s}^{-1})$
Interstitial	0.130	0.109
V_K	0.068	0.057
V_{Ta}	0.045	0.044
V_O	0.172	0.142

KTaO_3 cell, which is bound to an oxygen atom to form the $\text{O}\mu$ group. The Δ_{calc}^{eq} value for the V_O site is also close to the experimental one, but the probability of direct μ^+ trapping to this site is likely to be negligibly small because H^- is the only stable hydrogen species at the anion site of perovskite oxides.^{39,40} To form the muonic analogue of H^- , negatively charged muonium, each muon must acquire two electrons from the host lattice.⁶ However, such a process is unlikely to occur in the final stage of the μ^+ deceleration in the insulating environment.

Next, ZF- μ^+ SR spectra in the temperature range 3–25 K were fitted to $G_{\text{DKT}}(t; \Delta, \nu)$ with Δ fixed to $0.1322(12) \mu\text{s}^{-1}$ (Fig. 2(b)), which was determined by the simultaneous fit at 3.5 K. The temperature variation of ν is shown in Fig. 2(c) in an Arrhenius form. It appears to obey the Arrhenius law, $\nu(T) = \nu_0 e^{-E_a/k_B T}$, for two temperature ranges of 3.1–5.7 K and 7.4–25.1 K, with $\nu_0 = 1.3(2) \times 10^6$ and $3.3(2) \times 10^6 \text{ s}^{-1}$, and $E_a = 0.43(4)$ and $0.91(4) \text{ meV}$, respectively, where E_a is the activation energy. The values for the preexponential factor ν_0 are much smaller than the Debye frequency of KTaO_3 , $9.36 \times 10^{12} \text{ Hz}$,⁴¹ suggesting that the interstitial μ^+ diffusion in these temperature ranges is not of the classical over-barrier type. This may occur through incoherent quantum tunneling,¹² but we will not elaborate further on the mechanism of the low-temperature motion since quantum tunneling is beyond the scope of this paper.

B. Two-state model analysis for $75 < T < 300 \text{ K}$

We adopted a formulation of the 2S model by Lord *et al.* used for describing dynamical μ^+ behavior in ReO_3 .³⁷ It assumes that μ^+ starts at $t = 0$ in site 1 with a static relaxation rate Δ_1 and jumps at a rate ν between equivalent sites with an activation energy E_a . Then, μ^+ finds a trap (site 2) with a static relaxation rate Δ_2 at a probability c per jump, where the trapped μ^+ stays still for the rest of its lifetime. Given a static relaxation function $g_1(t) = e^{-\Delta_1^2 t^2}$ for site 1, the relaxation function $G_1(t)$ for μ^+ that jumps between site 1 and its equivalents and has never been trapped at site 2 is expressed as,

$$G_1(t; \nu, c, \Delta_1) = e^{-\nu(1-c)t} g_1(t; \Delta_1) + \nu(1-c) \int_0^t G_1(t-\tau) e^{-\nu(1-c)\tau} g_1(\tau; \Delta_1) d\tau.$$

TABLE II. Parameters used for or obtained from the 2S model analysis.

Temperature range (K)	Δ_1 (μs^{-1})	Δ_2 (μs^{-1})	E_a (eV)	ν_0 (s^{-1})	c
75-130	0.1322 (fixed)	0.0553(3)	0.099(4)	$1.0(6) \times 10^{13}$	0.027(4)
150-300	0.0553 (fixed)	0.0583(8)	0.216(8)	$1.3(7) \times 10^{12}$	0.007(1)

Using this together with a static relaxation function $g_2(t) = e^{-\Delta_2^2 t^2}$ for site 2, the total relaxation function $G_{2S}(t)$ including the contribution from μ^+ trapped at site 2 is given as,

$$G_{2S}(t; \nu, c, \Delta_1, \Delta_2) = e^{-\nu c t} G_1(t; \nu, c, \Delta_1) + \nu c \int_0^t G_1(\tau; \nu, c, \Delta_1) e^{-\nu c \tau} g_2(t - \tau; \Delta_2) d\tau. \quad (1)$$

We first performed a simultaneous fit of Eq. 1 to ZF- μ^+ SR spectra in the temperature range 75-130 K, assuming that the jump rate is subject to the Arrhenius law, $\nu(T) = \nu_0 e^{-E_a/k_B T}$. The result of the fit are shown in Fig. 4 with solid curves. Δ_1 was fixed to $0.1322 \mu\text{s}^{-1}$ through the fit since in this case site 1 should be associated with the interstitial bonding site for consistency with the DKT analysis. E_a and ν_0 for the interstitial μ^+ diffusion, c for finding defect A, and Δ_2 for μ^+ trapped at defect A were obtained from the fit, as shown in Table II. The value for E_a is close to that for interstitial μ^+ diffusion in other perovskites, such as SrZrO_3 ²⁵ and $\text{BaTiO}_{3-x}\text{H}_x$.²⁶ ν_0 for this temperature range is comparable to the Debye frequency in contrast to that for the low temperature regime below 25 K. This suggests that a change in the μ^+ hopping mechanism occurs from the possible quantum-tunneling type to a classical over-barrier type at around 75 K with increasing temperature. The Δ_2 value for μ^+ trapped in defect A is relatively close to the dipolar sum values for μ^+ at the cation vacancies in Table I, suggesting that defect A may be either V_K or V_{Ta} .

Equation 1 was also adopted to simultaneously fit ZF- μ^+ SR spectra in the temperature range 150-300 K, where the spectral shape is expected to primarily reflect μ^+ jumps between defect A and trapping in defect B. Here we assumed that the time that μ^+ spends at the interstitial sites during its diffusion from one trap to another is negligible in comparison with that spent in trapped states. In this analysis, site 1 is supposed to be defect A with its static relaxation rate of $0.0553 \mu\text{s}^{-1}$, which was determined from the 2S model analysis covering the temperature range 75-130 K. Therefore, we fixed Δ_1 to this value through the fit. The result of the fit is shown in Fig. 4 with solid curves. E_a and ν_0 for the intertrap μ^+ diffusion, c for finding defect B per intertrap jump, and Δ_2 for defect B were obtained from the fit, as shown in Table II. The value for E_a , which means the activation energy for escaping from defect A in this case, is significantly larger than that for the interstitial μ^+ diffusion as expected. ν_0 for this temperature range is close to the Debye frequency, suggesting that the trapping/detrapping

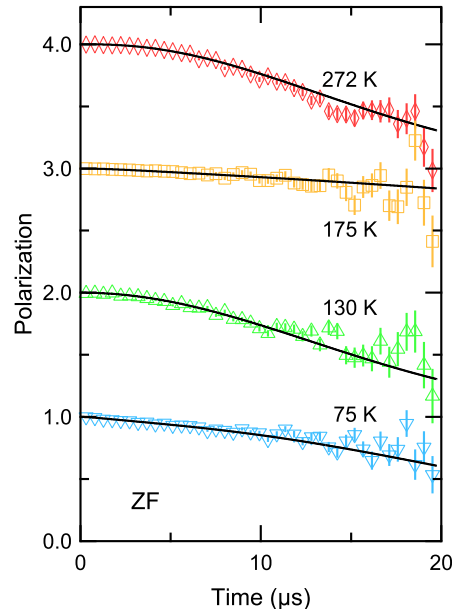


FIG. 4. ZF- μ^+ SR spectra at 75, 130, 175, and 272 K, compared to the result of the simultaneous fit of the two-state model (solid curves). For clarity, the base lines are vertically offset by +1 as the temperature increases.

process observed in this temperature range also occurs through the classical over-barrier hopping mechanism. The Δ_2 value for μ^+ trapped in defect B is also close to the dipolar sum values for μ^+ at the two cation vacancies in Table I, suggesting that defect B may be the other one of V_K and V_{Ta} that was not assigned to defect A.

The primary objective of this paper is to provide a semi-quantitative description of the long-range interstitial μ^+ diffusion above 75 K characterized by $E_a = 0.099(4)$ eV and $\nu_0 = 1.0(6) \times 10^{13}$ Hz, which suggests that it occurs through the classical over-barrier type hopping mechanism. In the following sections, we describe DFT calculations performed for this purpose.

IV. COMPUTATIONAL DETAILS

All calculations were performed within the DFT framework using the Quantum ESPRESSO package.^{42,43} The generalized gradient approximation using Perdew-Burke-Ernzerhof (PBE) exchange correlation functional was

adopted. Projector augmented-wave potentials with H(1s), K(3s, 3p, 4s), Ta(5s, 5p, 5d, 6s) and O(2s, 2p) valence states were used. Electron wave functions were expanded in plane waves with a cutoff of 70 Ry for kinetic energy and 600 Ry for charge density. The KTaO₃ structure was described using a $3 \times 3 \times 3$ supercell of the 5-atom cubic primitive cell. A H atom was placed at an interstitial position in the host supercell to model a dilute muon defect in the KTaO₃ lattice. While a $2 \times 2 \times 2$ supercell was used for similar calculations in Ref. 33 and 38, we more carefully employed the $3 \times 3 \times 3$ supercell to exclude the possibility of artificially stabilizing antiferro-distortions, which can occur in the $2 \times 2 \times 2$ supercell. Considering the amphoteric nature of the H defect, calculations were performed for defective supercells with $q = +1, 0$, and -1 , where q is the total charge of electrons and ions in the defective supercell. For the $q = +1$ or -1 cases, a uniform jellium background with an opposite charge was used to maintain charge neutrality.

Structure optimization. Brillouin zone sampling with a Monkhorst-Pack \mathbf{k} -point mesh of $2 \times 2 \times 2$ and Gaussian smearing with a broadening of 0.01 Ry were applied for structure optimization calculations. Atomic positions were relaxed while the lattice constant for the supercell was kept fixed at the calculated value of 12.024 Å for stoichiometric cubic KTaO₃, which was determined via full structure optimization. This value is consistent with the experimental lattice constant of 3.988 Å for the 5-atom primitive cell.⁴⁴ In all cases, atomic forces were converged to within 7.7×10^{-3} eV/Å.

Defect formation energy. The self-consistent field calculation for the optimized structure was refined using the optimized tetrahedron method⁴⁵ with a finer \mathbf{k} -point mesh of $5 \times 5 \times 5$ to avoid artifacts associated with the Gaussian smearing. The classical formation energy of the interstitial H defect with a charge q , $E_f(\text{H}^q)$, was calculated in accordance with a standard procedure described in Ref. 39 and 40:

$$E_f(\text{H}^q) = E_t(\text{H}^q) - E_t(\text{host}^0) - \frac{1}{2}\mu_{\text{H}_2} + q(\mu_{\text{VBM}} + E_F) + E_{\text{corr}}(\text{H}^q),$$

where $E_t(\text{H}^q)$ is the total energy of the defective supercell with a charge q , $E_t(\text{host}^0)$ is the total energy of a neutral host supercell, μ_{H_2} is the chemical potential of an H₂ molecule, μ_{VBM} is the chemical potential of the electron reservoir at the valence-band maximum, and E_F is the Fermi energy with reference to μ_{VBM} . $E_{\text{corr}}(\text{H}^q)$ is a small potential-alignment term for charged defective supercells,⁴⁶ which was determined from the difference in electrostatic potentials at an interstitial position about 10 Å away from the H defect.

Classical minimum energy paths. For the most stable H configuration determined by the above calculations, classical minimum energy paths (MEPs) between equivalent nearest neighbor H sites were searched using the nudged elastic band method³² with seven images. Brillouin zone sampling with a Monkhorst-Pack \mathbf{k} -point

mesh of $2 \times 2 \times 2$ and Gaussian smearing with a broadening of 0.01 Ry were applied. Atomic positions were relaxed with keeping the lattice constant fixed at the optimized value for stoichiometric KTaO₃ through iterations for finding the MEPs. A climbing image algorithm⁴⁷ was used to identify saddle points in the MEPs, which represent transition states (TSs) of corresponding H transfer events, and precisely compute classical barrier heights E_0 at the saddle points. In all cases, the norm of the force orthogonal to the path was converged to within 0.1 eV/Å.

ZPE-corrected μ^+ jump rates. The interstitial diffusion of H (pseudo) isotopes in the classical over-barrier hopping regime can be approximately explained using the harmonic transition state theory, which takes into account isotopic effects arising from zero-point vibrations within the harmonic approximation.³³ We adopted the double Born-Oppenheimer approximation for computing muon vibrational frequencies, which requires, in addition to the usual Born-Oppenheimer approximation being satisfied, that the vibrational motion of muons can be decoupled from that of other nuclei.³¹ This is justified because the muon's mass is much lighter than the mass of any other nucleus. In the double Born-Oppenheimer and harmonic approximations, ZPEs for muons in the initial (and final) equilibrium state (ES) and TS are expressed as $\sum_{i=1}^3 \frac{1}{2} \hbar \omega_i^{\text{ES}}$ and $\sum_{i=1}^2 \frac{1}{2} \hbar \omega_i^{\text{TS}}$, respectively, where ω_i^{ES} and ω_i^{TS} are harmonic vibrational angular frequencies for muons in the ES and TS. It should be noted that the sum for the TS runs over only two modes because the other mode is associated with a displacement along the MEP and therefore has an imaginary frequency at the saddle point. Consequently, a ZPE-corrected barrier height for the MEP with the classical barrier height E_0 is given as,

$$E_{\text{ZPC}} = E_0 + \sum_{i=1}^2 \frac{1}{2} \hbar \omega_i^{\text{TS}} - \sum_{i=1}^3 \frac{1}{2} \hbar \omega_i^{\text{ES}}. \quad (2)$$

According to the harmonic transition state theory, a ZPE-corrected muon jump rate k_{ZPC} can be calculated via the following equation,

$$k_{\text{ZPC}} = \frac{1}{2\pi} \frac{\prod_{i=1}^3 \omega_i^{\text{ES}} f(\hbar \omega_i^{\text{ES}}/2k_B T)}{\prod_{i=1}^2 \omega_i^{\text{TS}} f(\hbar \omega_i^{\text{TS}}/2k_B T)} \exp(-E_0/k_B T), \quad (3)$$

where $f(x) = \sinh(x)/x$.³³ At high temperatures, $f(\hbar \omega/2k_B T) \rightarrow 1$, so that eq. 3 reduces to the simple Arrhenius law with the activation energy of E_0 . At low temperatures,

$$k_{\text{ZPC}} \rightarrow (k_B T/h) \exp(-E_{\text{ZPC}}/k_B T), \quad (4)$$

where the preexponential factor $k_B T/h$ is in the order of 10^{12} Hz in the temperature range 75-300 K, which is close to the Debye frequency of KTaO₃. To calculate k_{ZPC} via eq. 3, ω_i s for the ES and TSs in all possible MEPs were computed using a density functional perturbation theory module in the Quantum ESPRESSO package within

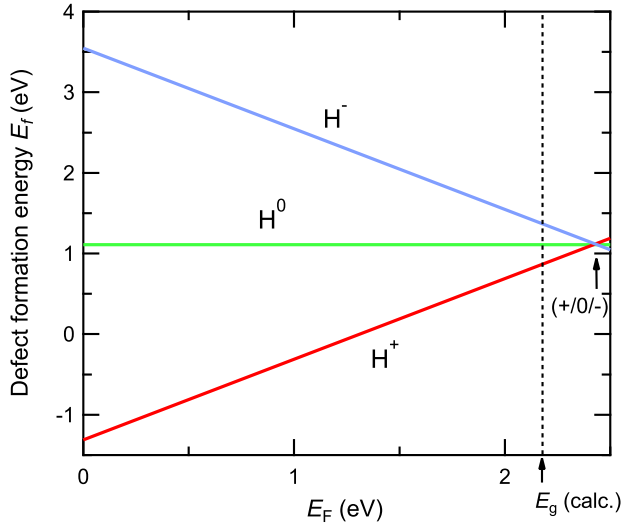


FIG. 5. Classical defect formation energies $E_f(H^q)$ for $q = +1, 0$, and -1 as functions of E_F . E_g is the bandgap calculated for a non-defective KTaO_3 lattice.

the framework of the double Born-Oppenheimer and harmonic approximations. In the density functional perturbation theory calculations, the muon was treated as a H isotope having the mass of $0.113m_p$, where m_p is the proton's mass.

V. COMPUTATIONAL RESULTS

A. Classical defect formation energy

Classical defect formation energies $E_f(H^q)$ for $q = +1, 0$, and -1 are obtained as functions of E_F , as shown in Figure 5. The three $E_f(H^q)$ lines cross at an $E(+/0/-)$ transition level in the conduction band. This means that the interstitial H always behaves as a shallow donor regardless of the position of E_F . All of the $q = +1, 0$, and -1 solutions have the OH group with its symmetry axis along the $\langle 001 \rangle$ direction, which is consistent with the previous DFT studies.^{33,38} It should be noted that in the $q = 0$ and -1 cases, excess electrons are not tightly bound to H, but are delocalized in the bottom of the conduction band. We carefully explored the possibility of electron localization using the PBE+ U method with a Hubbard U parameter of 5 eV for Ta $5d$ states, but this did not change the results. Therefore, all the solutions mean that the oxygen-bound protonic state is most stable in KTaO_3 .

The displacements of the K, Ta, and O atoms furthest from the proton at the equilibrium position in the $q = +1$ condition are as small as 0.008, 0.043, and 0.018 Å, respectively, with reference to corresponding atomic positions in the non-defective cubic lattice, confirming that the $3 \times 3 \times 3$ supercell is sufficiently large.

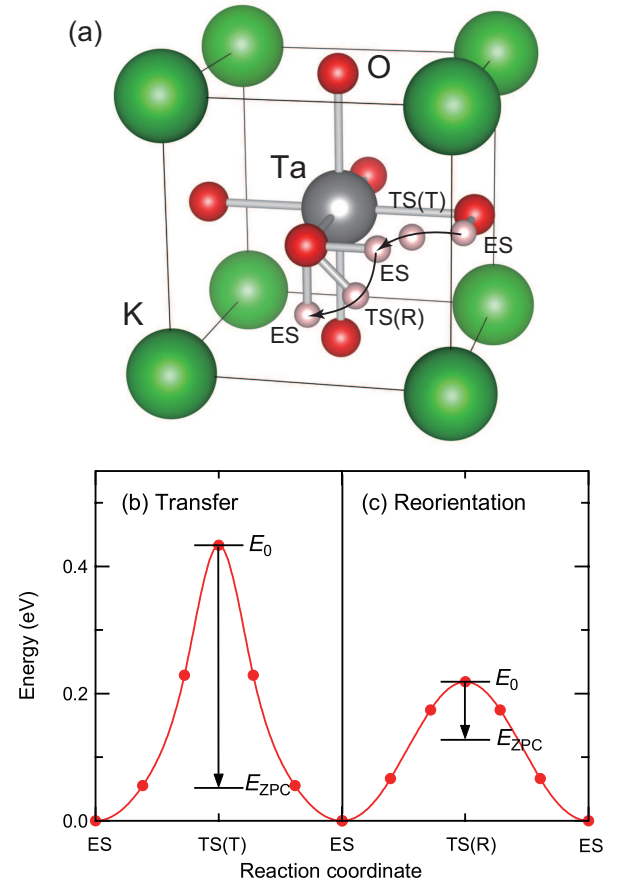


FIG. 6. (a) Schematic illustration of minimum energy paths for muon diffusion in KTaO_3 . (Bottom) One-dimensional energy profiles for muons moving along the transfer-type minimum energy path (b) and the reorientation-type minimum energy path (c), estimated using the nudged elastic band method. The reductions of the effective barrier heights due to the harmonic ZPE correction are represented with arrows.

B. Classical minimum energy paths for μ^+ by the nudged elastic band method

The global proton migration in the KTaO_3 lattice can be decomposed into two elementary steps of H hopping between equivalent ES sites,^{33,38} as shown in Fig. 6(a). One is the H/ μ transfer process between adjacent oxygen atoms via a bond-breaking transition state TS(T). The other is the H/ μ reorientation process around an oxygen atom via a transition state TS(R) without breaking the OH/O μ bond. One-dimensional energy profiles for H/ μ moving along the transfer-type and reorientation-type MEPs are shown in Fig. 6(b) and (c), respectively. The bottleneck process of the long-range interstitial diffusion is the H/ μ transfer ($E_0 = 0.43$ eV). The activation barrier height without the ZPE correction is approximately four times higher than the experimental value of ~ 0.1 eV.

TABLE III. Harmonic vibrational angular frequencies ω_i and corresponding harmonic ZPEs for muons in the ES, TS(T), and TS(R), together with the classical barrier heights E_0 obtained from the nudged elastic band calculations and the ZPE-corrected barrier heights E_{ZPC} for the two paths.

Muon's state	ω_1 (cm $^{-1}$)	ω_2 (cm $^{-1}$)	ω_3 (cm $^{-1}$)	ZPE (eV)	E_0 (eV)	E_{ZPC} (eV)
ES	10306	2528	2528	0.9375	-	-
TS(T)	5120	3844	3780i	0.5558	0.4333	0.0516
TS(R)	11054	2500	1733i	0.8403	0.2185	0.1213

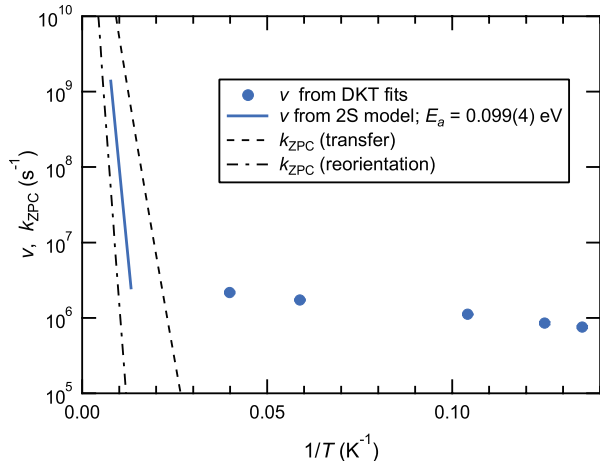


FIG. 7. Arrhenius plot for ν from the experiment and k_{ZPC} calculated with Eq. 3.

C. Zero-point energy corrected μ^+ jump rates

The parameters for the harmonic ZPE correction, ω_i and corresponding ZPEs for the ES, TS(T), and TS(R), are shown in Table III. A marked difference between ZPEs for the ES and TS(T) reflects the fact that the strong $\text{O}\mu$ bond associated with especially large ω_i s is temporarily broken in the TS(T). Consequently, the reduction in the effective barrier height due to the ZPE correction is more pronounced in the transfer-type path, resulting in a reversal of E_{ZPC} between the two paths [Table III and Fig. 6(b,c)]. The ZPE correction based on the harmonic transition state theory leads to the bottleneck barrier height of $E_{\text{ZPC}} = 0.1213$ eV for the reorientation-type path, which is close to the experimental value of ~ 0.1 eV for long-range interstitial μ^+ diffusion in KTaO_3 , as well as Sc-doped SrZrO_3 ²⁵ and $\text{BaTiO}_{3-x}\text{H}_x$.²⁶

A comparison between ν from the experiment and k_{ZPC} calculated with Eq. 3 is made in Fig. 7. The variation in the slope of $\nu(1/T)$ suggests that a change in the μ^+ hopping mechanism occurs from the possible quantum-tunneling type to the classical over-barrier type at around 75 K with increasing temperature. k_{ZPC} for the bottleneck path (dash-dotted line) approximately reproduces the temperature dependence of ν in the over-barrier hopping regime.

VI. DISCUSSION

KTaO_3 exhibits quantum paraelectric behavior at low temperatures, where the cubic structure and a virtual ferroelectric structure are nearly degenerate and the cubic symmetry is maintained via zero-point quantum fluctuations over these configurations. The atomic displacement in the virtual ferroelectric phase from corresponding atomic positions in the cubic phase was estimated from DFT calculations to be at most 0.026 Å.⁴⁸ This is one order of magnitude smaller than the local displacement of muon-neighboring atoms from our calculations, which reflects the chemical bonding state with muons. Therefore, the dynamical ferroelectric displacement associated with the quantum paraelectricity is likely to have only minor effects on muon kinetics, which involves the formation and breaking of the chemical bonds.

Since the potentials experienced by oxygen-bound protons in perovskite oxides generally reveal significant anharmonic terms along some directions,³⁹ it is not obvious whether the harmonic method can serve as a good approximation for describing ZPEs of muons in KTaO_3 . In particular, the adiabatic potentials corresponding to the $\text{O}\mu$ stretching vibrations (the ω_1 modes for ES and TS(R) in Table III) are highly asymmetric and anharmonic, and the deviation from the quadratic curve for the harmonic approximation should be significant except at the bottom of the potential wells.

A similar situation has been reported for vibrational modes of muons at around equilibrium positions in some fluorides.²⁸ In that paper, a comparison was made between harmonic ZPEs and those obtained by solving the Schrödinger equation for a muon in one-dimensional adiabatic potentials calculated along each vibration direction. Despite significant anharmonicity identified in some vibrational modes, there was surprisingly good agreement between the two sets of ZPEs.

We adopted the same strategy for KTaO_3 and solved the Schrödinger equation for a muon in adiabatic potentials corresponding to the seven muon vibrational modes in Table III with real frequencies using a finite-differences method. As a result, we obtained ZPEs of 0.9632, 0.5488 and 0.8621 eV for ES, TS(T), and TS(R), respectively, and the bottleneck barrier height of 0.1173 eV. The good agreement with corresponding harmonic values in Table III strongly suggests the validity of the harmonic approximation for describing the vibrational states of muons in

perovskite oxides.

The ZPE correction based on the harmonic approximation successfully accounted, at least semi-quantitatively, for the long-range interstitial μ^+ diffusion in KTaO_3 with the activation energy of ~ 0.1 eV. This relatively low-cost approach is probably also applicable to explaining that in Sc-doped SrZrO_3 and $\text{BaTiO}_{3-x}\text{H}_x$, which is characterized by similar activation energies.^{25,26} Furthermore, we can gain general insight into μ^+ states in oxides from the calculation results for KTaO_3 as described below.

The long-range interstitial μ^+ diffusion in oxides can usually be expressed as the combination of the transfer and reorientation-type hopping processes as in the case of KTaO_3 . The transfer-type process is characterized by the temporary breaking of the strong $\text{O}\mu$ bond in the TS(T), which results in a marked difference between ZPEs for the ES and TS(T). This can not only cause a significant reduction in the effective barrier height, but also change the ES for muons in extreme cases; from a viewpoint of ZPEs, muons prefer to stay in large interstitial or vacancy sites rather than forming the strong $\text{O}\mu$ bond at the conventional proton site adjacent to oxygen. This means that muons and hydrogen may be found in different stable sites due to the ZPE effect.

The barrier height for the transfer-type path between the conventional proton sites can vary widely depending on host crystal structures. When the proton sites are dense in the host lattice, as in the KTaO_3 perovskite, the barrier height can be relatively low in comparison with dilute cases; when the proton sites are far apart from each other, a higher energy for *completely* breaking the $\text{O}\mu$ bond (~ 5 eV, estimated from the average OH bond energy in H_2O) is expected to be required for transferring a muon from one site to another. Therefore, whether *global* muon diffusion becomes important in muon spin relaxation below room temperature should strongly depend on the crystal structure of host oxides.

On the other hand, the energy required for transferring a muon through the reorientation-type path is considered to be relatively independent of the crystal structure of host oxides because this process does not involve the temporary breaking of the $\text{O}\mu$ bond. Thus, provided that the crystal symmetry allows for such reorientation, the local motion of muons around oxygen may be characterized by a small barrier height of $0.1\sim 0.2$ eV. Since μ^+ SR is a local probe, even such local motion can cause significant changes in μ^+ SR spectra.^{23,24} Therefore, researchers who use μ^+ SR to study oxides need always keep in mind the possibility that muons can move even below room temperature when examining μ^+ SR data, and then carefully discuss physical properties of the oxides, such as magnetism and ionic conductivity.

It is worth mentioning that the above discussion on global and local motion of muons in oxides may also be applied to materials that involve elements with high electronegativity, such as C, N, S, Se, and halogens, which tend to create strong chemical bonds with implanted muons.^{49–51} It should also be noted that quantum tun-

neling of muons is beyond the scope of the DFT and harmonic transition state theory framework and higher-level calculations are necessary for correctly handling this phenomenon, such as using the *ab initio* path-integral molecular dynamics method.⁵²

The harmonic ZPEs for muons can be converted to those for protons under the double Born-Oppenheimer approximation by multiplying by the square root of the muon-proton mass ratio ($\sqrt{m_\mu/m_p} \sim 1/3$). From these scaled values, the bottleneck process for long-range diffusion of protons is inferred to remain the transfer type, with an activation barrier of about 0.3 eV. This value is considerably larger than that for muons, suggesting that the over-barrier-type diffusion of hydrogen (pseudo) isotopes in KTaO_3 exhibits a normal kinetic isotope effect. However, the justification for applying the double Born-Oppenheimer approximation to protons remains to be established, and more careful treatment may be necessary.

VII. CONCLUSIONS

In summary, we carried out μ^+ SR and DFT studies on μ^+ diffusion in the cubic perovskite KTaO_3 to gain a comprehensive understanding of the μ^+ diffusion in the perovskite oxide lattice. In the μ^+ SR experiment, we observed motional narrowing behavior, the evidence of interstitial μ^+ diffusion, at cryogenic temperatures. The μ^+ diffusion observed below room temperature was classified into two types; one is possibly the quantum-tunneling type, which is dominant below 75 K, and the other is the classical over-barrier type, which shows a major contribution at higher temperatures. The latter was indirectly identified through interactions between muons and defects, characterized by a small activation energy of ~ 0.1 eV. We successfully accounted, at least semi-quantitatively, for the small activation energy associated with the long-range interstitial μ^+ diffusion using the DFT and harmonic transition state theory framework. The significant reduction in the effective barrier height for the transfer-type μ^+ hopping path due to the ZPE correction is the key to understanding the small activation energy for KTaO_3 and other perovskite oxides.

We also obtained important insight into μ^+ states in other oxides from the calculation results for KTaO_3 . The effective barrier height for the transfer-type path can vary widely depending on the crystal structure of host oxides, whereas that for the reorientation-type path is expected to be relatively structure-independent and in the range of approximately 0.1 to 0.2 eV if the crystal symmetry allows for such reorientation. The low barrier height suggests that significant changes in μ^+ SR spectra can arise even below room temperature due to the local μ^+ motion regardless of whether the global motion is activated or not. This may prompt a revision of previous interpretations of μ^+ SR anomalies in some oxides, which have been claimed to be directly associated with the intrinsic

properties of the materials.

ACKNOWLEDGMENTS

We thank the staff of the J-PARC and PSI muon facilities for technical assistance and A. Koda, R. Kadono,

and K. Fukutani for helpful discussions. The DFT calculations were conducted with the supercomputer HPE SGI8600 in Japan Atomic Energy Agency. This research was partially supported by Grants-in-Aid (Nos. 23K11707, 21H05102, 20K12484, 20H01864, and 20H02037) from the Japan Society for the Promotion of Science.

-
- ¹ A. Amato, Heavy-fermion systems studied by μ SR technique, *Rev. Mod. Phys.* **69**, 1119 (1997).
 - ² S. J. Blundell, Muon-spin rotation studies of electronic properties of molecular conductors and superconductors, *Chem. Rev.* **104**, 5717 (2004).
 - ³ S. F. J. Cox, Muonium as a model for interstitial hydrogen in the semiconducting and semimetallic elements, *Rep. Prog. Phys.* **72**, 116501 (2009).
 - ⁴ A. Yaouanc and P. Dalmas de Reotier, Muon spin rotation, relaxation, and resonance: Applications to condensed matter (Oxford University Press, Oxford, 2010), 1st ed.
 - ⁵ W. Higemoto, Y. Aoki, and D. E. MacLaughlin, Spin and time-reversal symmetries of superconducting electron pairs probed by the muon spin rotation and relaxation technique, *J. Phys. Soc. Jpn.* **85**, 091007 (2016).
 - ⁶ T. U. Ito, W. Higemoto, and K. Shimomura, Negatively charged muonium and related centers in solids, *J. Phys. Soc. Jpn.* **89**, 051007 (2020).
 - ⁷ R. Feyerherm, A. Amato, A. Grayevsky, F. N. Gygax, N. Kaplan, and A. Schenck, Crystal electric field next to a hydrogen-like interstitial — μ^+ in PrNi_5 , *Z. Phys. B* **99**, 3 (1995).
 - ⁸ T. Tashma, A. Amato, A. Grayevsky, F. N. Gygax, M. Pinkpank, A. Schenck, and N. Kaplan, Electronic changes induced by μ^+ in PrIn_3 : Muon-spin-rotation observation and crystalline-electric-field model calculation, *Phys. Rev. B* **56**, 9397 (1997).
 - ⁹ F. N. Gygax, A. Schenck, G. Solt, P. C. Canfield, Muon site and local magnetic susceptibility in $\text{TmNi}_2\text{B}_2\text{C}$, *Physica B* **326**, 359 (2003).
 - ¹⁰ T. U. Ito, W. Higemoto, K. Ohishi, N. Nishida, R. H. Heffner, Y. Aoki, A. Amato, T. Onimaru, and H. S. Suzuki, Quantized hyperfine field at an implanted μ^+ site in PrPb_3 : Interplay between localized f electrons and an interstitial charged particle, *Phys. Rev. Lett.* **102**, 096403 (2009).
 - ¹¹ F. R. Foronda, F. Lang, J. S. Möller, T. Lancaster, A. T. Boothroyd, F. L. Pratt, S. R. Giblin, D. Prabhakaran, and S. J. Blundell, Anisotropic local modification of crystal field levels in Pr-based pyrochlores: A muon-induced effect modeled using density functional theory, *Phys. Rev. Lett.* **114**, 017602 (2015).
 - ¹² V. G. Storchak and N. V. Prokofev, Quantum diffusion of muons and muonium atoms in solids, *Rev. Mod. Phys.* **70**, 929 (1998).
 - ¹³ G. Alexandrowicz, T. Tashma, M. Socolovsky, A. Amato, A. Grayevsky, F. N. Gygax, M. Pinkpank, A. Schenck, and N. Kaplan, μ^+ hopping between magnetically labeled sites in PrIn_3 : “Kinematic” simulation and analytic treatment, *Phys. Rev. Lett.* **82**, 1028 (1999).
 - ¹⁴ T. U. Ito, W. Higemoto, K. Ohishi, N. Nishida, R. H. Heffner, Y. Aoki, H. S. Suzuki, T. Onimaru, H. Tanida, and S. Takagi, μ^+ diffusion in cubic f -electron compounds observed by high transverse field μ^+ SR, *J. Phys.: Conf. Ser.* **225**, 012021 (2010).
 - ¹⁵ R. Kadono, J. Imazato, T. Matsuzaki, K. Nishiyama, K. Nagamine, T. Yamazaki, D. Richter, and J.-M. Welter, Quantum diffusion of positive muons in copper, *Phys. Rev. B* **39**, 23 (1989).
 - ¹⁶ G. M. Luke, J. H. Brewer, S. R. Kreitzman, D. R. Noakes, M. Celio, R. Kadono, and E. J. Ansaldo, Muon diffusion and spin dynamics in copper, *Phys. Rev. B* **43**, 3284 (1991).
 - ¹⁷ J. Kondo, Diffusion of light interstitials in metals, *Physica B* **125**, 279 (1984).
 - ¹⁸ J. Kondo, Diffusion of light interstitials in metals, *Physica B* **126**, 377 (1984).
 - ¹⁹ K. Yamada, Diffusion of positive muon and orthogonality theorem, *Prog. Theor. Phys.* **72**, 195 (1984).
 - ²⁰ R. Hord, H. Luetkens, G. Pascua, A. Buckow, K. Hofmann, Y. Krockenberger, J. Kurian, H. Maeter, H.-H. Klauss, V. Pomjakushin, A. Suter, B. Albert, and L. Alff, Enhanced two-dimensional behavior of metastable T' - La_2CuO_4 , the parent compound of electron-doped cuprate superconductors, *Phys. Rev. B* **82**, 180508(R) (2010).
 - ²¹ A. Koda, H. T. Hirose, M. Miyazaki, H. Okabe, M. Hiraishi, I. Yamauchi, K. M. Kojima, I. Nagashima, J. Yamaura, Z. Hiroi, and R. Kadono, Coupled spin-charge-phonon fluctuation in the all-in/all-out antiferromagnet $\text{Cd}_2\text{Os}_2\text{O}_7$, *Phys. Rev. B* **100**, 245113 (2019).
 - ²² M. Månsson and J. Sugiyama, Muon-spin relaxation study on Li- and Na-diffusion in solids, *Phys. Scr.* **88**, 068509 (2013).
 - ²³ M. H. Dehn, J. K. Shenton, S. Holenstein, Q. N. Meier, D. J. Arseneau, D. L. Cortie, B. Hitti, A. C. Y. Fang, W. A. MacFarlane, R. M. L. McFadden, G. D. Morris, Z. Salman, H. Luetkens, N. A. Spaldin, M. Fechner, and R. F. Kiefl, Observation of a charge-neutral muon-polaron complex in antiferromagnetic Cr_2O_3 , *Phys. Rev. X* **10**, 011036 (2020).
 - ²⁴ M. H. Dehn, J. K. Shenton, D. J. Arseneau, W. A. MacFarlane, G. D. Morris, A. Maigné, N. A. Spaldin, and R. F. Kiefl, Local electronic structure and dynamics of muon-polaron complexes in Fe_2O_3 , *Phys. Rev. Lett.* **126**, 037202 (2021).
 - ²⁵ R. Hempelmann, M. Soetratmo, O. Hartmann, and R. Wäppling, Muon diffusion and trapping in proton conducting oxides, *Solid State Ionics* **107**, 269-280 (1998).
 - ²⁶ T. U. Ito, A. Koda, K. Shimomura, W. Higemoto, T. Matsuzaki, Y. Kobayashi, and H. Kageyama, Excited configurations of hydrogen in the $\text{BaTiO}_{3-x}\text{H}_x$ perovskite lattice associated with hydrogen exchange and transport,

- Phys. Rev. B **95**, 020301(R) (2017).
- 27 J. S. Möller, P. Bonfà, D. Ceresoli, F. Bernardini, S. J. Blundell, T. Lancaster, R. De Renzi, N. Marzari, I. Watanabe, S. Sulaiman and M. I. Mohamed-Ibrahim, Playing quantum hide-and-seek with the muon: Localizing muon stopping sites, Phys. Scr. **88** 068510 (2013).
 - 28 J. S. Möller, D. Ceresoli, T. Lancaster, N. Marzari, S. J. Blundell, Quantum states of muons in fluorides, Phys. Rev. B **87** 121108(R) (2013).
 - 29 R. B. L. Vieira, R. C. Vilão, A. G. Marinopoulos, P. M. Gordo, J. A. Paixão, H. V. Alberto, J. M. Gil, A. Weidinger, R. L. Lichti, B. Baker, P. W. Mengyan, and J. S. Lord, Isolated hydrogen configurations in zirconia as seen by muon spin spectroscopy and *ab initio* calculations, Phys. Rev. B **94**, 115207 (2016).
 - 30 T. U. Ito, Hydrogen-Ti³⁺ complex as a possible origin of localized electron behavior in hydrogen-irradiated SrTiO₃, e-J. Surf. Sci. Nanotech. **20**, 128 (2022).
 - 31 I. J. Onuorah, P. Bonfà, R. De Renzi, L. Monacelli, F. Mauri, M. Calandra, and I. Errea, Quantum effects in muon spin spectroscopy within the stochastic self-consistent harmonic approximation, Phys. Rev. Materials **3**, 073804 (2019).
 - 32 D. S. Sholl and J. A. Steckel, Density functional theory: A practical introduction (John Wiley & Sons, New Jersey, 2009).
 - 33 S. G. Kang and D. S. Sholl, First principles studies of proton conduction in KTaO₃, J. Chem. Phys. **141**, 024707 (2014).
 - 34 M. Berglund and M. E. Wieser, Isotopic compositions of the elements 2009 (IUPAC Technical Report) Pure Appl. Chem. **83**, 397 (2011).
 - 35 R. S. Hayano, Y. J. Uemura, J. Imazato, N. Nishida, T. Yamazaki, and R. Kubo, Zero- and low-field spin relaxation studied by positive muons, Phys. Rev. B **20**, 850 (1979).
 - 36 M. Borghini, T. O. Niinikoski, J. C. Soulié, O. Hartmann, E. Karlsson, L. O. Norlin, K. Pernestål, K. W. Kehr, D. Richter, and E. Walker, Muon diffusion in niobium in the presence of traps, Phys. Rev. Lett. **40**, 1723 (1978).
 - 37 J. S. Lord and W. G. Williams, Muon study of proton behaviour in rhenium trioxide, Solid State Ionics **145**, 381 (2001).
 - 38 M. A. Gomez, S. Jindal, K. M. Fletcher, L. S. Foster, N. D. A. Addo, D. Valentin, C. Ghenoiu, and A. Hamilton, Comparison of proton conduction in KTaO₃ and SrZrO₃, J. Chem. Phys. **126**, 194701 (2007).
 - 39 Y. Iwazaki, T. Suzuki, and S. Tsuneyuki, Negatively charged hydrogen at oxygen-vacancy sites in BaTiO₃: Density-functional calculation, J. Appl. Phys. **108**, 083705 (2010).
 - 40 Y. Iwazaki, Y. Gohda, and S. Tsuneyuki, Diversity of hydrogen configuration and its roles in SrTiO_{3-δ}, APL Mater. **2**, 012103 (2014).
 - 41 S. Bourgeat, R. Villar, S. Vieira, and V. A. Trepakov, Low temperature specific heat of KTaO₃ from 0.3K, Ferroelectrics **79**, 237 (1988).
 - 42 P. Giannozzi, S. Baroni, N. Bonini, M. Calandra, R. Car, C. Cavazzoni, D. Ceresoli, G. L. Chiarotti, M. Cococcioni, I. Dabo, A. Dal Corso, S. de Gironcoli, S. Fabris, G. Fratesi, R. Gebauer, U. Gerstmann, C. Gougousis, A. Kokalj, M. Lazzeri, L. Martin-Samos, N. Marzari, F. Mauri, R. Mazzarello, S. Paolini, A. Pasquarello, L. Paulatto, C. Sbraccia, S. Scandolo, G. Schlauro, A. P. Seitsonen, A. Smogunov, P. Umari, and R. M. Wentzcovitch, QUANTUM ESPRESSO: A modular and open-source software project for quantum simulations of materials, J. Phys.: Condens. Matter **21**, 395502 (2009).
 - 43 P. Giannozzi, O. Andreussi, T. Brumme, O. Bunau, M. Buongiorno Nardelli, M. Calandra, R. Car, C. Cavazzoni, D. Ceresoli, M. Cococcioni, N. Colonna, I. Carnimeo, A. Dal Corso, S. de Gironcoli, P. Delugas, R. A. DiStasio, A. Ferretti, A. Floris, G. Fratesi, G. Fugallo, R. Gebauer, U. Gerstmann, F. Giustino, T. Gorni, J. Jia, M. Kawamura, H.-Y. Ko, A. Kokalj, E. Küçükbenli, M. Lazzeri, M. Marsili, N. Marzari, F. Mauri, N. L. Nguyen, H.-V. Nguyen, A. Otero-de-la-Roza, L. Paulatto, S. Ponce, D. Rocca, R. Sabatini, B. Santra, M. Schlipf, A. P. Seitsonen, A. Smogunov, I. Timrov, T. Thonhauser, P. Umari, N. Vast, X. Wu, and S. Baroni, Advanced capabilities for materials modelling with Quantum ESPRESSO, J. Phys.: Condens. Matter **29**, 465901 (2017).
 - 44 A. Samara and B. Morosin, Anharmonic effects in KTaO₃: Ferroelectric mode, thermal expansion, and compressibility, Phys. Rev. B **8**, 1256 (1973).
 - 45 M. Kawamura, Y. Gohda, and S. Tsuneyuki, Improved tetrahedron method for the Brillouin-zone integration applicable to response functions, Phys. Rev. B **89**, 094515 (2014).
 - 46 C. Persson, Y.-J. Zhao, S. Lany, and A. Zunger, *n*-type doping of CuInSe₂ and CuGaSe₂, Phys. Rev. B **72**, 035211 (2005).
 - 47 G. Henkelman, B. P. Uberuaga, and H. Jónsson, A climbing image nudged elastic band method for finding saddle points and minimum energy paths, J. Chem. Phys. **113**, 9901 (2000).
 - 48 T. Esswein and N. A. Spaldin, Ferroelectric, quantum paraelectric, or paraelectric? Calculating the evolution from BaTiO₃ to SrTiO₃ to KTaO₃ using a single-particle quantum mechanical description of the ions, Phys. Rev. Research **4**, 033020 (2022).
 - 49 J. H. Brewer, S. R. Kreitzman, D. R. Noakes, E. J. Ansaldo, D. R. Harshman, and R. Keitel, Observation of muon-fluorine “hydrogen bonding” in ionic crystals, Phys. Rev. B **33**, 7813 (1986).
 - 50 K. Nishiyama, S. W. Nishiyama, and W. Higemoto, Asymmetric F-μ-F interaction of the muon in polyfluorocarbons, Physica B **326**, 41-45 (2003).
 - 51 T. Lancaster, S. J. Blundell, P. J. Baker, M. L. Brooks, W. Hayes, F. L. Pratt, J. L. Manson, M. M. Conner, and J. A. Schlüter, Muon-fluorine entangled states in molecular magnets, Phys. Rev. Lett. **99**, 267601 (2007).
 - 52 H. Kimizuka, S. Ogata, and M. Shiga, Mechanism of fast lattice diffusion of hydrogen in palladium: Interplay of quantum fluctuations and lattice strain, Phys. Rev. B **97**, 014102 (2018).